

Cite this article

Ramaiah G, Negawo TA, Baraki SY *et al.*
 Mechanical and tribological behavior of carbon-sisal fiber reinforced sandwich composites.
Emerging Materials Research,
<https://doi.org/10.1680/jemmr.25.00071>

Research Article

Paper 2500071
 Received 09/05/2025; Accepted 27/10/2025
 Emerald Publishing Limited: All rights reserved

Mechanical and tribological behavior of carbon-sisal fiber reinforced sandwich composites

**Gurumurthy Ramaiah**

Department of Textile Technology, Federal Technical and Vocational Training Institute, Addis Ababa, Ethiopia (Orcid:0000-0001-6698-117X) (corresponding author: voguru1@gmail.com)

Tolera A. Negawo

Department of Textile Technology, Federal Technical and Vocational Training Institute, Addis Ababa, Ethiopia (Orcid:0000-0003-1843-4440)

Senay Yacob Baraki

Department of Textile Technology, Federal Technical and Vocational Training Institute, Addis Ababa, Ethiopia (Orcid:0000-0003-2860-4247)

Robel Legese

Department of Textile Technology, Federal Technical and Vocational Training Institute, Addis Ababa, Ethiopia (Orcid:0000-0002-2533-0597)

Daniel Asfaw

Department of Textile Technology, Federal Technical and Vocational Training Institute, Addis Ababa, Ethiopia (Orcid:0000-0003-2898-8068)

Hailu Esayas Mekango

Department of Textile Technology, Federal Technical and Vocational Training Institute, Addis Ababa, Ethiopia (Orcid:0009-0004-6622-9059)



This research concerns the strength and robustness of sandwich composites from carbon and sisal fibers. These composites fulfill the need of the advanced manufacturing industry for strong materials as well as being robustly designed for comfort. Alkaline treatment was applied to sisal fibers to facilitate their bonding with the epoxy matrix. This improved the performance of this composite. The hybrid composites had superior mechanical properties compared with those from carbon fiber only. They were tested, and it was found that the maximum tensile strength was 193 MPa and impact absorption was 5.45 J. Tribological tests showed that the sliding friction coefficient ranged from 0.525 to 0.71, which means that the surface is better where wear is lower. It was optimized and fine-tuned some key processing parameters using a Taguchi L8 orthogonal array. The four- to six-layer composites consisted of a 50%–60% epoxy matrix and a 6.5 mm-thick composition. Characterization methods, including differential scanning calorimetry, Fourier transform infrared spectroscopy, and scanning electron microscopy, supported the fibers to be dispersed well and bonded strongly in-between surfaces and formulated to be stable at high temperatures. These eco-friendly hybrid composites are highly strong and work well in the military, aerospace, and automotive environments. They

AQ: 1 establish long-term high-performance composite materials with natural fibers in state-of-the-art structural design.



Keywords: carbon fiber/composite materials/hybrid composites/mechanical properties/sisal fiber/tensile strength/tribology/UN SDG 9: Industry, innovation and infrastructure/UN SDG 12: Responsible consumption and production

1. Introduction

Fiber-reinforced polymer (FRP) composites have gained widespread attention in aerospace, automotive, marine, and civil engineering applications due to their high strength-to-weight ratio, resistance to corrosion, wear, and fatigue, and design flexibility.^{1,2} Conventional synthetic composites, such as carbon fiber reinforced polymers (CFRPs), offer excellent mechanical and tribological properties but are expensive and pose environmental challenges during disposal.³ On the contrary, natural fiber composites – such as those reinforced with sisal, jute, or flax – are renewable, biodegradable, and lightweight, making them suitable for environmentally sustainable applications. However, natural fibers typically suffer from limitations such as lower mechanical performance, poor moisture resistance, and variability in quality due to their biological origin.^{4,5}

The emerging concept of hybrid composites, combining synthetic and natural fibers in a single matrix system, offers a

promising route to engineer materials with enhanced performance and environmental compatibility.^{6,7} In particular, carbon-sisal hybrid composites blend the stiffness and strength of carbon fibers with the eco-friendliness and low cost of sisal fibers. These hybrid systems aim to achieve a balance between performance and sustainability, which is crucial for lightweight structural applications requiring both mechanical durability and a reduced ecological footprint.⁸

Despite several studies on synthetic or natural fiber composites, limited research has focused on their synergistic combination in structured architectures, such as sandwich composites.⁹ Moreover, many previous studies suffer from uncontrolled fiber dispersion, poor interfacial bonding, and inconsistent fabrication methods that limit reproducibility and scalability.¹⁰ There is a pressing need to optimize fiber treatment, orientation, and resin content to develop repeatable and reliable hybrid composites.

In this study, the design and development of sisal-carbon epoxy hybrid composites using a controlled hand lay-up technique. The sisal fibers are locally sourced and pretreated to improve bonding, while carbon fabrics are introduced as reinforcement layers to boost mechanical and tribological performance.^{11–13} The sandwich composite structure – with a lightweight core and strong outer layers – offers improved energy absorption, wear resistance, and stiffness, making it suitable for applications such as car bumpers, aerospace fairings, and marine panels.

A design of experiments (DOE) approach is used to systematically investigate the influence of fiber layer configuration, number of plies, and resin content on tensile strength, flexural strength, and coefficient of friction (COF). This quantitative modeling allows performance prediction and optimization, bridging the gap between experimental testing and real-world applications.

The novelty of this work lies in combining synthetic and natural fibers into a hybrid architecture, optimizing the composite parameters using statistical methods, and simultaneously evaluating mechanical and tribological behavior under practical loading conditions. The insights from this study contribute to the development of cost-effective, high-performance, and environmentally friendly materials for next-generation transportation and structural applications.

2. Materials and methods

This research focuses on the development of a hybrid polymer matrix composite with the help of carbon fabric, sisal fiber, and epoxy resin. PAN-based plain weave carbon fabric (0.1–0.68 thick) provides high tensile strength (4000 MPa+) and Young's modulus (230–240 GPa), suitable for structural use. Sisal fiber, a natural reinforcement that is environmentally friendly, provides a tensile strength of 468–700 MPa and a modulus of 9.4–22 GPa. The combination of synthetic and natural fibers yields a cheap composite material that is reinforced. Epoxy resin and hardener guarantee compatibility and good attachment with the fibers as well. Their densities (1.15–1.24 g/cm³) hold the structure. Mold release agents, such as wax or acetone, avoid sticking during curing. The removal of the laminate after post-curing helps in surface finish and strength. The composite allows for the balance of sustainability and high performance.

The resin system requires exact mixing techniques for proper curing and functional operation. Both workers and facilities must obey strict safety measures, including gloves and adequate ventilation requirements. When mixing resin with hardener at temperatures between 24°C and 30°C, both components should be poured accurately, while complete mixing ensures there will be no formation of micro-bubbles, which prevent proper curing. The required tools for consistent composite material creation and testing include beakers along with mixing sticks, rollers, brushes, weighing scales, scissors, and universal testing machines (UTMs).

2.1 Extraction and alkali treatment of sisal fibers

Sisal fibers (Figure 1) have to be extracted and treated chemically before their use in the composites. Extraction entails drying of leaves and manually or mechanically removing fibers. Unprocessed fibers include lignin, hemicellulose, waxes, and oils, which prevent bonding with resins. For this reason, alkali treatment (mercerization) is applied. This process is responsible for free of unwanted impurities, roughening the surface, or improving the fiber wettability. It severs internal bonds, thus precipitating more reactive cellulose (Equation 1). Treated fibers are more compatible with polymer matrices. This improves its mechanical performance and makes sisal a more efficient reinforcement.⁴



where the hydroxyl groups of the fiber react with sodium hydroxide (NaOH) to form alkoxide groups. This strengthens the bond of the composite between fiber and matrix.

Ten percent of sodium hydroxide was used for the alkali treatment of sisal fibers prepared by blending into 4 l distilled water. The sisal fibers were soaked in the alkali solution at room temperature for 24 h for successful surface modification. After post-treatment, fibers were washed with distilled water to eliminate any trace amount of sodium hydroxide as well as diffused impurities. Washing continued until a pH of 7 was achieved after removal from alkali (Figure 2). The fibers were dried in the sun for 2 days to remove the moisture. Composites were made from the treated fibers, which were also cut into different lengths after drying. This kind of alkali treatment significantly increased the mechanical properties of the composites without affecting the natural quality of the fibers. It also improved the intermolecular bonding of the fibers to the epoxy matrix, which gave it structure and function.⁵



Figure 1. Sisal fiber plant



Figure 2. (a) Dry sisal fiber and (b) alkali-treated sisal fiber

2.2 Carbon/sisal/epoxy hybrid composite preparation

The manufacture of sisal/carbon/epoxy hybrid composites is performed using a structured hand lay-up.^{6,8} To initiate the process, a $200 \times 70 \times 7 \text{ mm}^3$ metal mold is made in accordance with the schematic representation shown in Figure 3. For the composite development process, there must be the placement of thin plastic sheeting and then an external mold release agent coating, such as wax or acetone. In the curing of epoxy resin, the mold surface prevents sticking with this barrier. The steps to design a composite begin by laying out layers of treated sisal fibers and carbon fabric in alternating layers to achieve a layer ply configuration. A particular epoxy resin-to-hardener ratio is blended together to a sandy consistency and brushed skillfully or rolled it so as to apply it evenly for full fiber saturation. Layers are built in a sequential manner beginning from carbon fiber and sisal fiber till the required thickness is achieved. During curing, the layered structure will be under pressure. A tool for eliminating bubbles left from the final resin application is employed afterwards. These kinds of composites show an improvement in the mechanical and tribological properties.⁷

2.3 Experimental design and optimization approach

Two-level DOE in a minimally tested way selects our interest's processing parameters^{8,9} (Table 1). However, techniques such as

Table 1. Factors and levels

Factor	Factor name	Minimum	Maximum
A	Fabric thickness: mm	3.0	6.5
B	Epoxy matrix concentration: %	50	60
C	Number of fabric plies: n	4	6

factorial design, Taguchi design, response surface methodology, and mixture design increase levels of accuracy and efficiency. The Taguchi method (L8 orthogonal array (2^3)) studies three important factors in eight runs. The design is utilized to determine the impact of input variables on the mechanical and tribological properties of the hybrid composite.¹⁰ It will help create appropriate conditions for better material behavior (Table 2).

The goal of the DOE analysis is to systematically investigate and optimize the effects of key processing parameters on the mechanical and tribological performance of the carbon/sisal hybrid composites. Each parameter is selected based on its expected influence on fiber-matrix interaction, composite strength, and durability. This approach helps identify the most critical factors, their interactions, and optimal settings, ensuring a more efficient and targeted composite development process.

In the fabrication of the sandwich composite, a carbon woven fabric was strategically placed on the outer layers to provide high strength and stiffness, while a sisal fiber mat was used as the core or inner layer to enhance toughness and reduce weight. Given that the total areal density (GSM) of the composite is 250 g/m^2 , and considering the epoxy matrix constituted either 50% or 60% of the total weight, the remaining 40%–50% (i.e. 100–150 gsm) represents the combined fiber content. The equal distribution of fiber content between the outer and inner layers, approximately half of this fiber weight (50–75 gsm), is attributed to the carbon fabric on the surfaces, with the rest being the sisal fiber mat in the core. This layered arrangement effectively balances mechanical

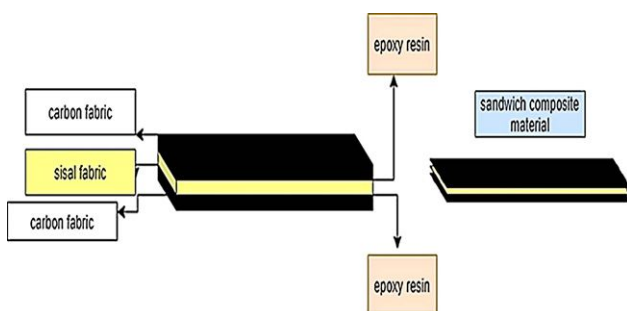


Figure 3. Architecture of sisal/carbon/epoxy sandwich composites

Table 2. Taguchi L9 orthogonal array used for development and testing of carbon/sisal hybrid composite

Sample no	Fabric thickness: mm	Epoxy matrix conc: %	No of plies	Tensile strength: MPa	Flexural strength: MPa	Impact energy: J	Sliding friction coefficient: μ
1	3	50	4	130	110	3.52	0.525
2	3	50	4	130	115	3.6	0.53
3	3	60	6	180	150	4.44	0.65
4	3	60	6	182	160	4.6	0.71
5	6.5	50	6	193	170	5.2	0.56
6	6.5	50	6	190	172	5.45	0.55
7	6.5	60	4	180	165	5.1	0.6
8	6.5	60	4	180	160	5.1	0.61

performance and cost-efficiency, making it suitable for lightweight structural applications.

2.4 SEM, FTIR, and DSC test methods

Carbon/sisal fiber-reinforced composites were analyzed for their structural, chemical, and thermal properties utilizing advanced techniques of characterization. High-resolution surface imaging and analysis of the failure pattern of the surface were done at the Center for Nano Science and Engineering, with the help of TESCAN MIRA 3 FE-SEM. The element of composition was investigated by means of the Bruker Quantax 200 EDS system. Plasma cleaning of the XEI Evactron system removed hydrocarbon contaminants and thus improved the clarity of the image. These tools were helpful in a detailed study of fiber bonding and surface morphology. Surface analysis in detail is crucial for the interpretation of mechanical behavior and failure mechanisms in hybrid composites.

Differential scanning calorimetry (DSC) and Fourier transform infrared spectroscopy (FTIR) were used in the analysis of chemical interaction and thermal properties in the composite. FTIR at CeNSE with PerkinElmer Spectrum 1000 helped identify functional groups and chemical bonds between sisal fibers and the polymer or carbon matrix, indicating that the chemical treatments applied to the sisal fibers to enhance compatibility result in effective treatments. Measuring thermal properties such as melting point, glass transition temperature, and crystallinity was done by way of the PerkinElmer DSC 8000. Its double furnaces guaranteed accurate and consistent results. These analyses determined how thermally stable the composite was and its application at high temperatures.¹⁴ When combined, these methods improve comprehension and functionality of the carbon/sisal composites for use in engineering.

2.5 Mechanical and tribological test methods

Mechanical and tribological tests determine the appropriateness of carbon/sisal fiber-reinforced composites as a structural application.¹⁵⁻¹⁷ Standard tensile, flexural, and impact tests resolved to resistance to stress, bending, and shock. Tensile and flexural samples have the same dimensions, and impact tests are conducted based on Izod/Charpy specifications. Performance is a function of

fiber-matrix bonding and alignment.^{18,19} Through the use of tribological tests, wear and friction are tracked; useful for engineering and automotive uses.

2.5.1 Tensile strength test (ASTM D3039)

The ultimate tensile strength is the maximum tension a material can take before failure occurs. This very valuable property and Young's modulus (stiffness) are valuable for the analysis of the tolerance of the material performance. The test for tensile was done using ASTM D3039 on a 200 kN electromechanical WAW-100 UTM (Figure 5). Specimens, 190 mm long, 25 mm wide, and 4.5 mm thick, were tested with the average of each three samples. Failure usually occurred at mid-length along the gauge length, where there was initial damage at the grip areas, which meant stress concentration or failure of the grip. Matrix cracking gradually led to fiber breakage, uncontrollable crack propagation, and loss of structural completeness.²⁰ Tensile loading made these fiber-reinforced composites brittle.

2.5.2 Flexural strength test (ASTM D790)

The testing in flexural strength evaluates the material's possibility to retain its shape against the bending load, and this is an important feature of the composite to have under the flexural loading conditions. For this study, ASTM D790 standards were used to determine the three-point bending characteristics of the composites made of carbon/sisal sandwich composites. 75 mm support span and the central load were tested on 190 mm \times 25 mm \times 4.5 mm samples. From the tests, failure began with matrix cracking, which led to fiber breakage in the tension zone, where maximum stress was reported. Characteristic failure sequence in fiber-reinforced composites is: the matrix then fails due to the weight until the breaking of reinforcing fibers. Further testing resulted in loss of load-bearing ability and its gradual decrease in stiffness.²¹ The results are relevant when considering the flexural resistance required by structural applications, they are useful for an understanding of the bending performance of carbon/sisal composites.

2.5.3 Impact test (ASTM D256)

The Charpy impact tester and ASTM D256 is a known techniques for evaluating the toughness of the material in terms of energy

absorbed in high-speed fracture. It assists in exposing a material's ability to withstand sudden forces and its tendency for a ductile-to-brittle transition behavior. This is a very common, straightforwardly performed and interpreted test, which does not give absolute readings. In this study, samples were of ASTM D256 dimensions. 65 mm × 12.7 mm × 5 mm. The size and geometry of the specimen affect the initiation and propagation of fracture, thus impacting strength.

2.5.4 Tribological test

The tribological behavior of the carbon/sisal composite at ambient temperature was conducted using the dry pin-on-disk wear test (ASTM G99).¹⁸ The force of pin pressing was generated by pressing the stationary pin with a flat button sized 3 mm and a rounded contact surface into a rotating disk so that the latter felt as if it was sliding against the disk. Using cut composite samples, wear tests were performed with forces of 10–15 N and linear velocities of 0.15–0.35 m/s. The tribometer was maintained at a constant level of friction and wear process for accurate results.^{22,23} ASTM G99-95 standards for cylindrical pins of 4 mm and 12 mm long were used for the wear tests in order to calculate the sliding coefficient of friction.

2.5.5 Wear test method and ASTM standard

This test is perfectly established in that it is considered a standard test with different names. A test for wear resistance of materials, a test for composite, literally is a language to describe the pin-on-disk method as per ASTM G99. In this test, a stationary cylindrical pin is pressed forcefully into a turning disc under a load and sliding speed within limits that shall bring into effect abrasion of contact surfaces by friction and a process of removal of material as a disc is tested against a rotating surface, the rate of wear and the COF can be measured. For the obtained results to be stable and consistent, such important parameters as applied load, sliding distance, and the conditions of the environment are sharply controlled. It is preferred to use this technique because it is easy, accurate, and applicable to actual sliding wear cases. ASTM G 65 (dry sand/rubber wheel) and ASTM D3702 (thrust washer test) are the rest of the standards used for the specific wear types, while ASTM G99 still remains the most prevalent. Wearing causes dimensional reduction in materials is stated in volume loss that is generally in cubic millimeters (mm³). The rate of wear is provided by decomposing the volume lost by the product of the normal force and sliding distance, from Equation 2.

$$\text{Wear Rate (W)} = \text{Volume Loss} / (\text{Normal Load} \times \text{Sliding Distance}). W = V/L.F$$

where V is the volume loss (in mm³), L is the sliding distance (in meters), F is the applied normal load (in newtons).

Since wear rate rises as volume loss rises, it implies that more material is wasted over the same distance of sliding. It is possible because of increased friction or harder materials or increased loads. This relation also assists us in assessing how the performance of a material degrades over time when applied in a special manner.

3. Results and discussion

3.1 Surface characterization

Carbon-sisal composites, when observed under SEM, reveal distinct fibers running across the sample, each maintaining its natural construction pattern (Figure 8(a)). The microstructure formed by combining sisal's natural fibers with carbon reinforcement displays woven or embedded fibers that offer structural support within the matrix (Figure 8(b)). The resulting composite structure is irregular due to the varying origins of sisal fibers and synthetic carbon fibers (Figure 8(c)). SEM imaging highlights three main material variations: differing fiber dimensions, orientation patterns, and distribution, which contribute to the visual characteristics of the composite. Fiber-matrix interaction is a key factor in determining the composite's overall performance, with strong bonding between fibers and matrix enhancing mechanical strength.

Further observations in Figure 4(a) show the smooth, relatively uniform surface of the carbon fibers, highlighting their continuous, cylindrical structure. Figure 4(b) displays the sisal fibers, characterized by their rougher, more irregular, and fibrillated surface, often seen as bundles. Figure 4(c) appears to be a fractured surface or cross-section of the composite material, likely showing the intricate intertwining or integration of both carbon and sisal fibers within a matrix, demonstrating the internal structure and interaction points.

The scanning electron microscopy (SEM) images are used to measure the quality of the fiber-matrix interface to observe the bonding status and even the potential gap or regions of separation that may result in material failure. Fiber pull-out patterns and interfacial gaps give an indication of failure points; smooth surfaces represent successful matrix infiltration (Figure 4). A combined SEM imaging with energy-dispersive spectroscopy (EDS) analysis gives an extensive view of the composite's structure and elemental composition. Before SEM examination, samples were coated with conductive layers, for example, gold, to avoid charging effects. EDS spectra display signals from carbon and oxygen, the latter of which are produced from cellulose and lignin of sisal fibers. This integrated SEM-EDS method helps to determine the structural integrity as well as the distribution of compound elements of the composite material.

3.2 SEM energy-dispersive X-ray spectroscopy analysis

The carbon-sisal composite sample under observation (Figure 5) exhibits clear peaks for gold (Au), carbon, and oxygen (O) in its

F4

F5

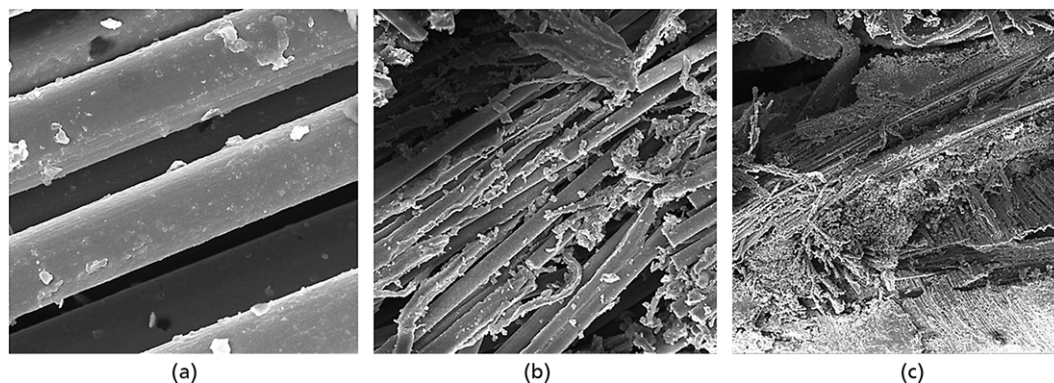


Figure 4. (a) SEM micrograph of carbon fabric; (b) sisal fibers; and (c) composite material

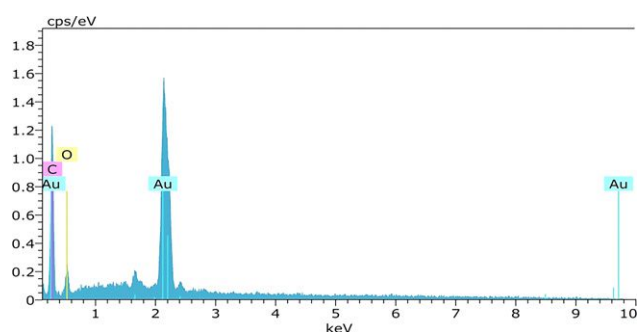


Figure 5. Energy-dispersive X-ray spectroscopy (EDS) spectrum

energy-dispersive X-ray spectrum (EDS). The gold peaks are produced by the gold sputtering process, a normal procedure to improve the surface conductivity for SEM imaging. The carbon in the composite corresponds to carbon fiber and sisal, both of which contain carbon. The oxygen peak is probable in lignin and cellulose from sisal and possible surface oxidation. The height and areas of peaks relative will help measure elemental composition in the studied area, confirming the inhomogeneity of the sample.

3.3 Elemental composition from spectrum

From the EDS analysis (Table 3), gold is the most concentrated by weight (78.39% wt), indicating the sample is gold-coated. By comparison, carbon has an extremely high atomic percentage (73.02 at%); it can be said that the material probably has carbon compounds, such as polymers or organic compounds. Oxygen (O)

occurs in lower concentrations (2.86 wt%, 8.36 at%), which may indicate surface oxidation or the existence of organic functional groups. High percentages of error for carbon and gold indicate that there is some variation in the sample or inhomogeneity. The unnormalized total of 80.68 wt% suggests that lighter elements are present that cannot easily be detected by EDS (e.g. hydrogen or nitrogen) may be present. Overall, the composition suggests a composite or a coated structure, likely a gold-coated organic or a carbon-based material.

3.4 FTIR spectra of carbon/sisal composite

The curve for a carbon/sisal composite (red line) and carbon fiber (black line) from the FTIR spectra (Figure 6) clearly indicates that the two have different chemical functional groups present due to their absorption of the infrared light at different levels. The x -axis

F6

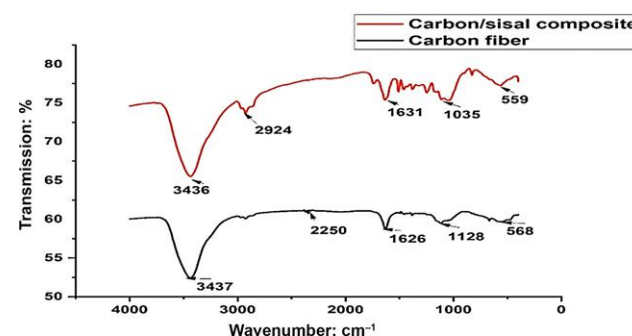


Figure 6. FTIR of carbon/sisal composite materials

Table 3. Elemental composition analysis of carbon-sisal composite

Element	X-ray series	Unnormalized conc.: wt%	Normalized conc.: wt%	Atomic conc.: at%	Error (3σ , wt%)
Gold (Au)	M-series	63.24	78.39	18.62	7.33
Carbon (C)	K-series	15.13	18.75	73.02	6.81
Oxygen (O)	K-series	2.31	2.86	8.36	1.57
Total	—	80.68	100.00	100.00	—

reveals wavenumber (cm^{-1}), and the y -axis gives percentage transmission. FTIR spectroscopy determines functional groups in a sample by observing the vibrational frequencies of bonds in the molecules in the sample. A lower value of transmission implies that the sample's functional groups are absorbing a lot of light, providing information about the chemical groups present in the material.

The primary advantages of incorporating sisal into composites, as indicated by FTIR analysis, stem from its unique chemical composition, which introduces reactive functional groups (hydroxyl, carbonyl, and ether). These groups are crucial for enhancing the compatibility and adhesion between the sisal fibers and the matrix, leading to improved mechanical properties of the final composite. In addition, sisal's natural origin contributes to the sustainability and cost-effectiveness of the material, offering a renewable and often cheaper alternative to purely synthetic reinforcements.

The FTIR spectra (Figure 6) clearly show the difference between the carbon/sisal composite and carbon fiber. Both spectra demonstrate a broad absorption band in the range of 3436–3437/ cm corresponding to the O–H stretching vibration of moisture or manufacturing processes. The composite displays improved peaks at 2924/ cm (C–H stretching in cellulose and lignin from sisal), 1631/ cm (C=O stretching in hemicellulose and lignin), and 1035/ cm (C–O stretching in cellulose), which are omitted or poorly defined in the carbon fiber spectrum. The absorbance spectrum of carbon fiber confirms weak absorbance peaks at 2250/ cm (it means nitrile groups or carbonization process impurities), 1626/ cm (C=C stretching), and 1128/ cm (C–O or Si–O on the surface). The two spectra have common peaks at 559 and 568/ cm , which may be attributed to metal-oxygen bonds or inorganic materials. The FTIR analysis identifies the distinctive chemical composition of the

composite by establishing distinct variations between the functional groups found in sisal and carbon fibers.

3.5 Differential scanning calorimetry

Thermal responses during the heating and cooling cycles of the carbon/sisal composite are disclosed by its DSC thermograms (Figure 7). During the heating of the composite, the DSC curve (having temperature as the x -axis, $^{\circ}\text{C}$, and heat flow as the y -axis, (W)) has major thermal events (Figure 7(a)). A first endothermic peak at 26°C shows the evaporation of moisture from the hydrophilic sisal fibers.

A large endothermic area, centered on 157°C , matches the hemicellulose breakdown in the lignocellulosic framework of sisal. Further heating then gives two interesting exothermic peaks around 227°C and 270°C , which indicate decomposition of cellulose and lignin components. These exothermic events indicate the initiation of a high-order classification of thermal decomposition and structural transformations in response to the organic matter breakdown and transformation in the carbon matrix.

In the cooling cycle, the carbon/sisal composite continues to have distinctive thermal behavior. From 270°C , the heat flow goes up, and a wide exothermic transition at about 156°C implies molecular reorganization/re-crystallization in the composite. This reformation of bonds is caused by the stabilization of partially degraded lignocellulosic and carbon structures into new arrangements. Furthermore, a mild thermal event around 25°C indicates the possibility of a glass transition or relaxation process in the organic matrix (Figure 7(b)). Overall, the DSC evidenced the full picture for the thermal stability, decomposition paths, and structure transformations in the carbon/sisal composite over a wide range of temperatures and pointed out both of its degradation schemes and the possibility of reorganization processes under thermomechanical stress.

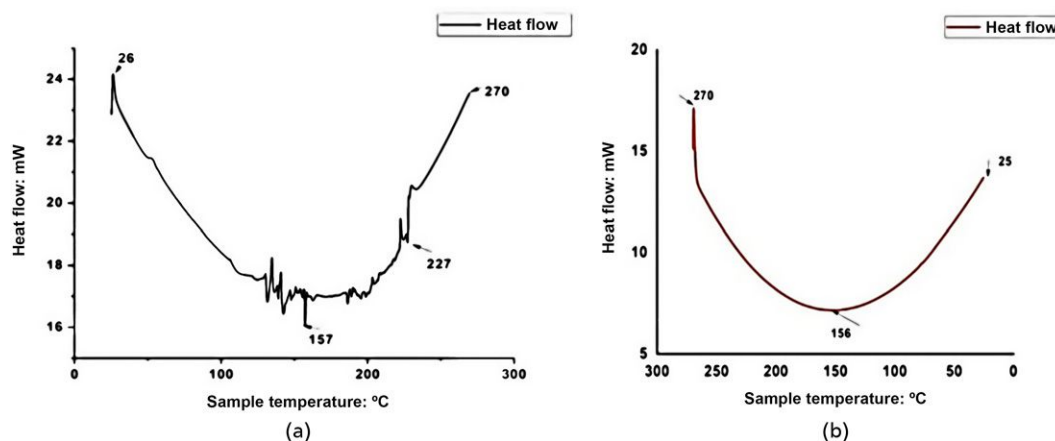


Figure 7. DSC plot for carbon/sisal composites: (a) heating curve and (b) cooling curve

3.6 Mechanical and tribological properties of carbon/sisal composites

3.6.1 Tensile strength (MPa)

F8

The tensile strength graph (Figure 8) and Table 2 for eight samples show a clear relationship with variations in fabric thickness, epoxy matrix concentration, and the number of plies. Samples 1 and 2, with 3 mm thickness, 50% epoxy, and 4 plies, recorded the lowest tensile strength of 130 MPa, indicating a basic structural configuration. Increasing the epoxy concentration to 60% and the number of plies to 6 in Samples 3 and 4 (still 3 mm thick) significantly improved tensile strength to 180 and 182 MPa, respectively. The highest tensile strength values were observed in Samples 5 and 6 (193 and 190 MPa), which had increased fabric thickness (6.5 mm) and 6 plies, despite maintaining 50% epoxy. Samples 7 and 8 also had 6.5 mm thickness and 60% epoxy but fewer plies (4), leading to a moderate tensile strength of 180 MPa. This indicates that both fabric thickness and number of plies positively influence tensile strength, while epoxy concentration plays a secondary role. Overall, optimal tensile performance is achieved with higher fabric thickness and more plies.

The bar chart, with standard deviation error bars, enhances understanding of the carbon/sisal composite's tensile strength by illustrating both mean performance and data variability. Samples 1 and 2 display notable variation, but Samples 3–8, especially Sample 5 (193 MPa with a small error bar), show impressive consistency and high mean tensile strengths. These values are competitive with, or even surpass, many common synthetic polymer composites (100–300 MPa) and certain light alloys.

3.6.2 Flexural strength (MPa)

F9

The bar graph (Figure 9) shows the flexural strength of eight carbon/sisal composite samples, indicating the influence of

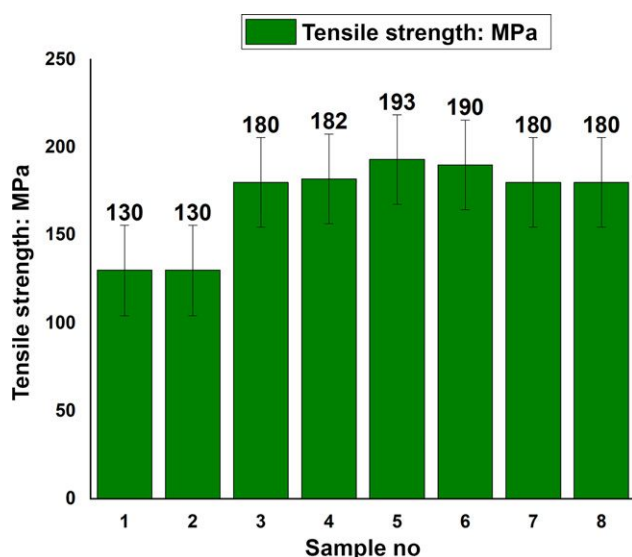


Figure 8. Bar graph of tensile test of different samples

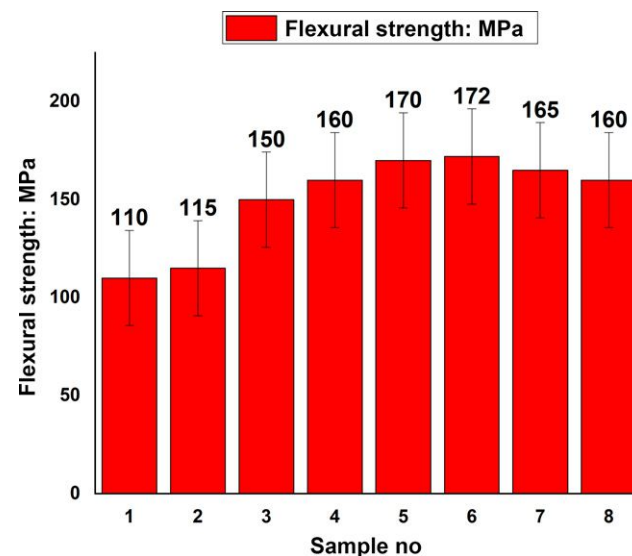


Figure 9. Bar graph of flexural test of different samples

fabrication variables on bending resistance. Samples 1 and 2, fabricated with 3 mm fabric, 50% epoxy, and 4 plies, have the weakest strengths (110 and 115 MPa). Strength is considerably improved in Samples 3 and 4 (150 and 160 MPa) as the number of plies is increased from four to six and the epoxy concentration is increased to 60% without increasing the fabric thickness.

Samples 5 and 6 have the highest flexural strengths (170 and 172 MPa) due to 6.5 mm fabric, and 6 plies and 50% epoxy, which underscores the relevance of ply numbers and fabric thickness. Samples 7 and 8 have the same thickness fabric and 60% epoxy, but only 4 plies, showing a drop of strength marginally (165 and 160 MPa), meaning more plies diminish performance for more epoxy.

The bar graph (Figure 9) illustrates the flexural strength (MPa) of carbon-sisal composites across eight samples, with error bars representing the standard deviation. Compared with literature values for natural fiber composites, which typically range from 80 to 150 MPa (Bledzki and Gassan, 1999), the results, particularly for Samples 4–8, demonstrate superior mechanical performance, validating the effectiveness of carbon-sisal reinforcement strategies. These results show that flexural strength is sensitive to fabric thickness and ply count, while ply concentration plays a secondary but significant role.²⁴ Optimal bending performance requires thoughtful tuning of all three parameters and increases structural reliability and strength of composite applications.

3.6.3 Impact energy (J)

The bar graph (Figure 10) demonstrates the effect of energy absorption of eight carbon/sisal composite samples and ultimately explaining how the fabrication parameters affect the material's reaction to sudden loads. Samples 1 and 2 with 4 plies, 3 mm

F10

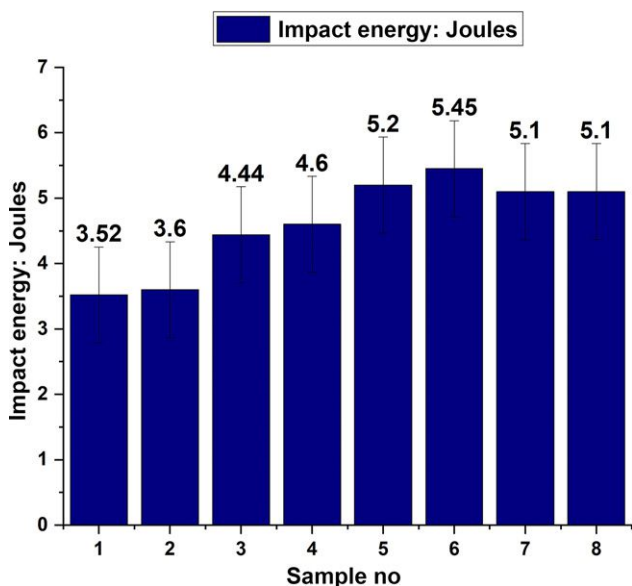


Figure 10. Bar graph of impact energy(J) of different samples

fabric thickness, 50% Epoxy recorded the lowest absorption (3.52 and 3.6 J), thus weak impact resistance. Samples 3 and 4 were improved to 4.44–4.6 J by increasing ply number to 6 and the epoxy content to 60% while the fabric thickness stayed the same. Samples 5 and 6 appeared with 6 plies, thicker at 6.5 mm fabric, and 50% epoxy at the highest resistance, 5.2 and 5.45 J, highlighting the need for more plies and thicker fabric. While Samples 7 and 8 had the same fabric thickness and 60% epoxy, they had 4 plies and slightly lower absorption (5.1 J), confirming that ply number and fabric thickness are more dominating than epoxy conc. alone. In general, optimal impact energy is achieved by balancing fabric thicknesses, plies, and epoxy matrix concentration.

Compared with literature^{25–37} on conventional natural fiber composites such as flax or jute, which often exhibit lower impact strengths (~2–4 J), these hybrid composites demonstrate enhanced energy absorption. The novel aspect here lies in the strategic hybridization of high-strength carbon fiber with sustainable sisal fiber, achieving a balance between mechanical performance and eco-friendliness.^{34,36} The synergy significantly boosts impact resistance while reducing reliance on synthetic fibers, making the material ideal for lightweight and semi-structural applications. Error bars plotted on each column represent the standard deviation among repeated samples. The results show good consistency and reliability across the composite sets.

3.6.4 Sliding friction (μ)

F11 The bar graph (Figure 11) represents the COF of eight samples of carbon/sisal composites. It demonstrates how the parameters in the fabrication apply to the way the samples react when they touch each other. Samples 1 and 2 have the lowest COF (0.525 and 0.53). They also have a thinner layer of fabric (3 mm), lower



Figure 11. Test samples of carbon/sisal composites after testing

epoxy matrix concentration (50%), and fewer plies (4), hence they are less resistant to motion. Samples 3 and 4 have significantly higher coefficients (0.65 and 0.71) because the level of plies and percentage of epoxy were increased to 60% and fabric thickness remained the same. This implies that these changes are highly inflating friction. Samples 5 and 6 have middle coefficients and keep the same 50% epoxy concentration and 6 plies, but with the thicker fabric (6.5 mm), they are less frictional than Samples 3 and 4.

Compared with literature values, typical synthetic composites (e.g. carbon or glass fiber reinforced epoxy) often exhibit lower COF values (~0.3–0.5), while natural fiber composites such as jute or

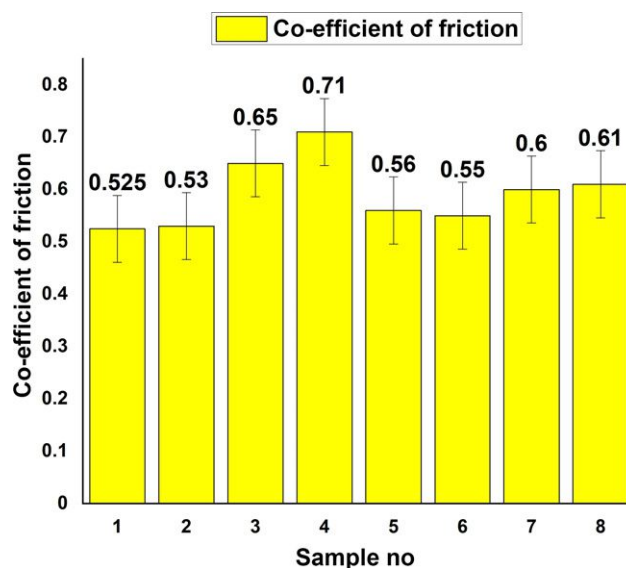


Figure 12. Bar graph of coefficient of friction (sliding friction) of different samples

hemp range between 0.45 and 0.65. This suggests that the hybrid sisal/carbon configuration not only preserves structural integrity but also improves frictional performance, making it suitable for wear-critical applications such as brake pads or sliding components. The novelty lies in combining the high strength of carbon fiber with the inherently rough, high-friction surface of sisal, offering a sustainable alternative with enhanced tribological behavior. The plotted error bars, representing standard deviation, show moderate variability, particularly in Samples 3 and 4, which reflects the influence of fiber orientation and surface characteristics. Overall, the results confirm reliable testing and fabrication consistency.

Finally, Samples 7 and 8 have friction values of 0.6 and 0.61, which are higher than Samples 5 and 6 but lower than the peak seen in Samples 3 and 4. These samples also use the thicker fabric, but they only have 4 plies and a level of 60% epoxy. These results show that the thickness of the fabric does affect how it frictionally behaves, but the concentration and number of plies of epoxy have a bigger impact on the COF in carbon/sisal composites.

3.6.5 Wear rate

The well-known equation $WR = \text{Volume Loss}/(\text{Force} \times \text{Sliding Speed})$ is a wear rate equation, which has been widely used in tribology, for determining the wear behavior of various materials under various loading conditions and sliding conditions. This equation describes the volumetric loss from wear as a function of the applied load and sliding speed, which both impact the tribological outcome of the material. It is largely referred to in research articles and technical analysis on the wear resistance of composites, metals, and polymers in frictional contact.^{35,37,38}

The relatively high fiber reinforcement content of the carbon/sisal/epoxy material system is revealed by the composite density of 1.60 g/cm^3 , which contributes to increased mechanical performance. According to the rule of mixtures, this density can be obtained with approximate volume fractions of 60% carbon fiber, 25% sisal fiber, and 15% epoxy resin. Carbon fiber, being denser, at about 1.75 g/cm^3 , has a greater effect on the final density of the composite, while sisal, being denser, at about 1.45 g/cm^3 as well as epoxy, at about 1.20 g/cm^3 , play a role in complementing the structure.

This fibrous composition implies that the material is intended for use in applications that require a combination of strength with lightweight, which are enhanced by the predominance of carbon fiber and wear resistance, and a sustainable route to cost-saving is provided through the sisal fiber. The approximate volume loss for all eight experiments using a composite density of 1.60 g/cm^3 is shown in Table 4.

The wear rate analysis of the carbon/sisal/epoxy composite shown in Table 5 indicates a decreasing trend as the sliding speed and applied load are increased. The greatest wear rates were in

Table 4. Tribological properties of carbon-sisal composite

Experiment	Weight loss: g	Volume loss (mm^3) = (weight loss \times 1000) \div 1.60
1	0.0146	$0.0146 \times 1000 \div 1.60 = 9.13$
2	0.0107	$0.0107 \times 1000 \div 1.60 = 6.69$
3	0.0133	$0.0133 \times 1000 \div 1.60 = 8.31$
4	0.0138	$0.0138 \times 1000 \div 1.60 = 8.63$
5	0.0119	$0.0119 \times 1000 \div 1.60 = 7.44$
6	0.0135	$0.0135 \times 1000 \div 1.60 = 8.44$
7	0.0110	$0.0110 \times 1000 \div 1.60 = 6.88$
8	0.0131	$0.0131 \times 1000 \div 1.60 = 8.19$

Table 5. Wear rate of carbon-sisal composite

Experiment	Volume loss: mm^3	Speed: m/s	Force: N	Wear rate: $\text{mm}^3/\text{N}\cdot\text{m/s}$
1	9.13	0.15	10	6.09
2	6.69	0.20	12	2.79
3	8.31	0.25	13	2.56
4	8.63	0.30	14	2.05
5	7.44	0.35	15	1.42
6	8.44	0.15	10	5.63
7	6.88	0.20	12	2.87
8	8.19	0.25	13	2.52

Experiments 1 and 6, of 6.09 and $5.63 \text{ mm}^3/\text{N}\cdot\text{m/s}$, respectively, for lower sliding speeds (0.15 m/s) and loads (10 N). This implies that at the low load and speed regime, the material encounters higher localized friction and a lack of stability, which leads to increased volume loss. On the contrary, the minimum wear rate of $1.42 \text{ mm}^3/\text{N}\cdot\text{m/s}$ from experiment 5 is associated with the highest speed (0.35 m/s) and the highest load (15 N), thereby suggesting that an increased operating condition may favor better surface conformity and coating deposition, hence reducing wear. The medium, moderate, and steady wear rates in Experiments 2–4 and 7–8 (between 2.05 and $2.87 \text{ mm}^3/\text{N}\cdot\text{m/s}$) represent a balanced performance on the medium scale. Overall, the composite shows increased wear resistance at higher speeds and forces, validating its applicability in dynamic tribological applications.

3.7 Optimizing sliding friction in composites using the Taguchi method

The selection of signal-to-noise (S/N) ratios in the Taguchi optimization method depends on the intended operational behavior of the studied performance characteristics. Among the three primary S/N ratios, we have ‘Smaller-the-Better’, ‘Larger-the-Better’, and ‘Nominal-the-Best’. Depending on the response property, the ‘Smaller-the-Better’ principle for analyzing tribological properties, including sliding friction and wear rate measurement, is the better option.^{39,40} The optimization technique works to minimize these performance measures by reducing both friction and material damage, thus improving composite functional longevity. The ‘smaller-the-better’ S/N ratio calculation uses this formula (Equation 3).

T4

T5

3. $S/N = -10 \log_{10} (1/n \sum y_i^2)$

The analysis enables determining control parameter configurations that minimize wear while reducing friction manifestations. When evaluating traits with better performance at higher values, the ‘Larger-the-Better’ rule provides optimal parameters to measure.⁴¹ The ‘Smaller-the-Better’ method to minimize the friction coefficient delivers the most effective tribological performance improvement during sliding friction scenarios.

T6 Table 6 shows average sliding friction coefficients for each of the control parameters at two levels, where lower values demonstrate improved tribological performance. The ‘Delta’ values show how influential each parameter is in determining sliding friction, with the concentration of epoxy matrix having the most significant effect ($\Delta = 0.1012$), number of plies next ($\Delta = 0.0512$), and the fabric thickness having the least effect ($\Delta = 0.0237$). The epoxy concentration is identified as the major determinant of friction, and the lowest epoxy level (Level 1) produces the least average friction value (0.5413), likely attributed to lesser surface adhesion. The impact of creating more plies (Level 2) on fiber interaction leads to high friction, while fabric thickness has a minimal contribution to the change in frictional behavior.⁴² Overall, the most effective low-friction combination is a low epoxy concentration, fewer plies, and thinner fabric, yielding the best composite performance for non-slip applications.

What distinguishes the main effects S/N ratios plot from the main effects mean is what they are applied to and how they should be interpreted. The S/N ratio plot considers the average performance and the variability. It aims at finding the factor levels contributing to the process stability and its resistance to noise, especially when we talk about ‘smaller is better’ or ‘larger is better’ rules. On the contrary, the means plot will only give the average response (similar to average sliding friction) at each level of a factor, but not the variability. The means plot indicates what levels of a factor give the best mean result. The S/N plot, however, is preferable in locating conditions that give consistent performance as conditions vary.

The objective is to reduce the S/N ratios by examining the sliding friction behavior in the carbon/sisal hybrid composites using three critical influencing parameters: fabric thickness, epoxy matrix concentration, and number of plies. The analysis indicates that an increase in fabric thickness from 3.0 to 6.5 mm produces better S/N ratios and reduces sliding friction, which features improved tribological performance with lower surface resistance (Figure 13). On

F13

Table 6. Response table for means (sliding friction)

Parameter	Level 1	Level 2	Delta	Rank
Fabric thickness: mm	0.6038	0.5800	0.0237	3
Epoxy matrix conc: %	0.5413	0.6425	0.1012	1
Number of plies	0.5663	0.6175	0.0512	2

the contrary, when the epoxy matrix concentration is increased from 50% to 60% the respective S/N ratio reduces drastically; while mean sliding friction increases due to the diminished level of fiber interaction and increased surface bonding. Similarly, when the number of plies is raised from four to six, the S/N ratio is also reduced, indicating an increase in fiber interfaces and also the stacking stiffness, and therefore, higher friction is introduced. The main effect plot indicates that mean sliding friction is decreasing with thicker fabrics, but increasing with both increased epoxy concentration and with more plies (Figure 14).⁴³ In general, the best tribological performance characterized by the lower sliding friction is reached with the use of thicker fabric, lesser epoxy content, and less plies in the composite structure.

F14

The two-dimensional (2-D) contour (Figure 15) and three-dimensional (3-D) surface profile (Figure 16) taken together provide a comprehensive picture of the intricate association between the fabric thickness, COF, and number of plies in carbon/sisal composites. On the 2-D contour plot, fabric thickness is shown along the x-axis, COF along the y-axis, and the number of plies is represented as a color gradient, with green tones indicating less than 4 plies and darker shades indicating more than 6 plies (Figure 15). The emergent visualization shows that thinner fabrics paired with higher ply counts often leave the friction coefficients higher, highlighting the significance of ply on the frictional

F15

F16

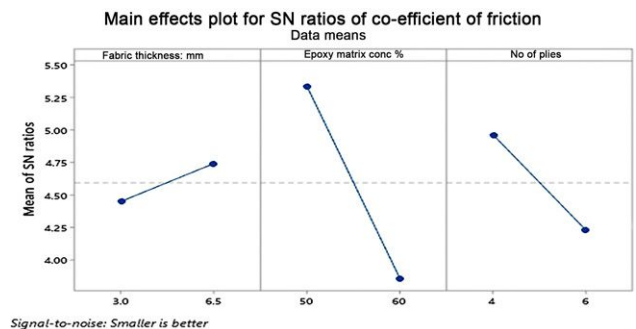


Figure 13. Main effect plot for SN ratio-sliding friction as response

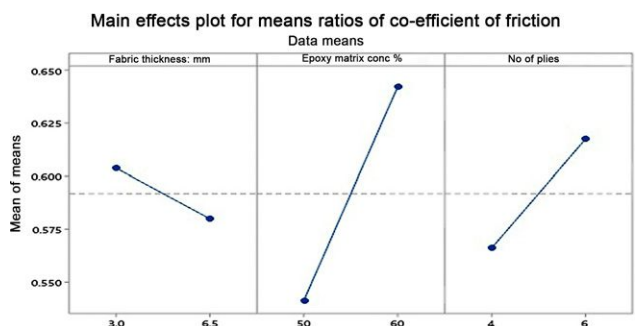


Figure 14. Main effect plot for means-sliding friction as response

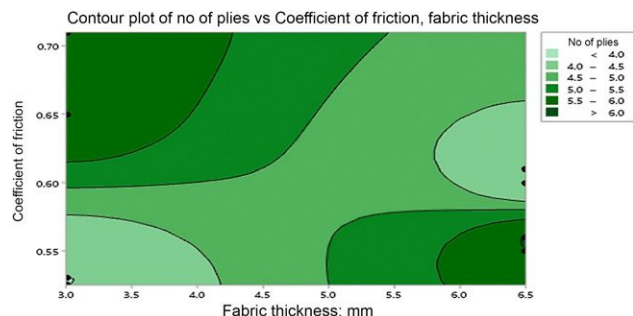


Figure 15. 2-D contour plot for sliding friction response

3-D surface plot of Co-efficient of friction vs No of plies and Fabric thickness

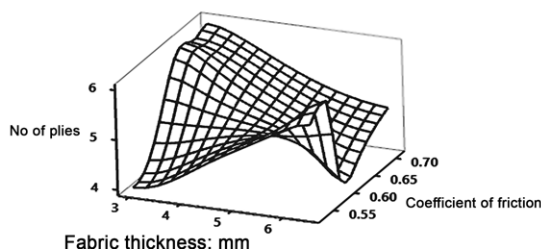


Figure 16. 3D surface plot for sliding friction as response

strength, especially in less thick materials. The 3-D surface plot (Figure 16) adds further visual to this understanding through fabric thickness on the x -axis, friction coefficient on the y -axis, and number of plies on the z -axis, thus showing a nonlinear and curved relationship among the three parameters.⁴⁴ These graphical tools are essential in determining the role of the composite structure in targeted tribological applications, for example, optimizing the brake linings or clutch systems.

3.7.1 Optimal parameters and response

A 3 mm fabric thickness, 50% of the epoxy matrix mixture, and 4 plies give the best settings for predicting the performance of a carbon/sisal composite in the area of sliding friction. These settings were chosen because they can minimize friction the most. 3 mm fabric thickness ensures that the load is evenly distributed, the 50% epoxy matrix concentration is moderate enough to obtain a good bond and to minimize friction. Using 4 plies helps maintain the solidity of the composite structure without much increasing its slipperiness (this is, by using fewer plies, it becomes less slippery). This mix is extremely effective in the areas where a low level of friction is required, that is, in the case of clutches or brake linings, where performance and wear resistance play a major role.

3.8 Carbon-sisal and glass fiber composites: Performance comparison

In terms of strength-to-weight ratio and impact resistance, carbon-sisal hybrid composites perform better than traditional glass fiber

composites in both mechanical and tribological tests. The given data showed that the tensile strength of carbon-sisal composites ranged from 130 to 193 MPa. Better performance was seen when the epoxy concentration was higher and the fabric thickness was higher. In the same way, flexural strength went up and reached 172 MPa. The results show that carbon-sisal laminates, especially when the matrix content and ply count are increased, have the same or better mechanical integrity than regular glass fiber composites. These composites usually have tensile strengths between 150 and 250 MPa and flexural strengths between 200 and 300 MPa, depending on the formulation and orientation.

Results indicate that carbon-sisal composites exhibited higher energy absorption (up to 5.45 J) while achieving better friction coefficients (0.525–0.71), indicating enhanced performance in active conditions. The stiffness and strength of glass fiber composites remain high, yet these materials feature poor resistance to breakage and provide weak protection against impact forces. Carbon-sisal composites combine carbon fibers that provide stiffness with sisal fibers, which deliver toughness into one hybrid material. Such composites demonstrate potential for installation within vehicle structures and semi-structural components, which include car door panels and seat backs, as well as bumper reinforcements and engine covers, and trunk liners. These parts benefit from this composite, which provides both lightness and increased resistance through impact and environmentally-friendly disintegration.⁴⁵ Alternative automotive applications should consider carbon-sisal composites because they offer affordability, combined with workability, along with environmental friendliness at reasonable costs.

It is important to note that this comparison is generalized, as the mechanical and tribological properties of composites are highly influenced by several factors, including fiber architecture, volume fraction, surface treatment, and the specific manufacturing process employed. The cited literature (Table 7) provides more detailed insights into the configurations and processing techniques used and supports the demonstrated superiority of carbon/sisal composites over glass fiber composites in various contexts.

The hybrid carbon/sisal composite exhibits mechanical strength on par with glass fiber composites, while offering better impact resistance and reduced wear rate due to the synergistic behavior of carbon's stiffness and sisal's damping capability. Its COF is also lower than that of pure sisal composites, approaching that of carbon fiber composites, suggesting good surface interaction under tribological loading conditions.

4. Conclusion

This research shows that carbon-sisal hybrid composites can attain mechanical properties similar to the conventional glass fiber composites if the matrix concentration and ply number are maximized. The tensile strength peaked at 193 MPa, and flexural strength at 172 MPa – numbers which fall in the normal range for glass fiber

Table 7. Comparison of mechanical properties of carbon/sisal composites

Composite type	Tensile strength: MPa	Flexural strength: MPa	Impact strength: kJ/m ²	Wear rate: mm ³ /N·m	COF	Reference
Glass fiber/epoxy	320–450	450–550	35–50	$3.5\text{--}5.0 \times 10^{-4}$	0.30–0.35	30,28,31
Sisal fiber/epoxy	80–150	100–160	15–25	$6.0\text{--}8.0 \times 10^{-4}$	0.40–0.50	25,26
Carbon fiber/epoxy	500–900	600–900	50–80	$2.0\text{--}3.0 \times 10^{-4}$	0.25–0.30	33
Carbon/sisal hybrid composite	320–500	400–600	40–60	$2.5\text{--}3.5 \times 10^{-4}$	0.28–0.33	27,29,32

composites (150–250 MPa tensile and 200–300 MPa flexural). This validates the fact that the incorporation of natural sisal fibers remains strong. One of the major advantages that was noted was the high impact energy absorption of 5.45 J, so much higher than most of the available glass fiber composites. The addition of sisal fibers increases toughness by minimizing crack propagation and delaying failure under a dynamic load.

Tribological testing also indicated desirable performance with friction coefficients from 0.525 to 0.71. These values are characteristic of stable surface interphasing's and high resistance to sliding and abrasive forces. Such properties make the composite ideal for parts subjected to repeated motion, friction, or impact. The resistance to vibrations and wear increases the usability of the created products to the high demands of environments. In general, carbon-sisal composites provide a viable alternative with competitive mechanical/tribological benefits.

The hybrid composite, which is comprised of carbon fiber stiffness and sisal fiber toughness, is suitable for various automotive parts, such as door panels, seat backs, bumper reinforcements, engine covers, and trunk liners. Such composites have advantages such as light weight, increased shock absorption, and biodegradability, which follow current automotive aims for sustainability and performance. Moreover, substituting some carbon fiber with natural fibers reduces material prices while not affecting critical mechanical strength. The composites are simple to fabricate and cost-effective for mass production. They are therefore attractive for structural as well as semi-structural use in vehicles.

Environmentally, the use of sisal promotes circular economy objectives as it minimizes the ecological implications during production and end use. This sustainable character of the composites makes them a potential green alternative for high-performance segments. Improved fiber surface treatments, modified stacking sequences, and the use of sophisticated compatibilizers are possibilities for further improvements. Such measures may improve interfacial bonding and thus improve mechanical and thermal properties. Such evolutions would extend the range of conditions applicable to carbon-sisal composites to even more severe environments.

Finally, carbon-sisal sandwich composites are a nature-friendly and technically viable alternative to synthetic fiber-reinforced composites. Their progress is a step toward utilizing natural fibers

in standard composite engineering. This assists in achieving a good balance between the cost and performance, and the environment.

Conflict of interest

The authors declare that they have no conflict of interest.

Author contributions

Gurumurthy Ramaiah: conceptualization, research framework, methodology, analysis, writing original draft, software, supervision, writing, reviewing, and editing; Tolera A. Negawo: experimental procedures, laboratory evaluation; Senay Yacob Baraki: material preparation functions, coordinated tasks; Robel Legese: review of literature, discussion, and analysis; Daniel Asfaw: data visualization and correspondence tasks; Hailu Esayas Mekango: experiments, data analysis, analytical evaluations, and statistical interpretations.

Data availability

The data that support the findings of this study are available from the corresponding author upon reasonable request.

Acknowledgements

The authors would like to express their sincere gratitude to the Federal Technical and Vocational Training Institute, Addis Ababa, Ethiopia, for providing the opportunity and support to conduct this research. The authors also extend their appreciation to the Centre for Nano and Soft Matter Sciences (CeNS), Arkavathi, Survey No. 7, Shivanapura, Dasanapura Hobli, Bengaluru – 562162, for offering access to their testing facilities used for the characterization and analysis of the carbon/sisal composites.

REFERENCES

- Faruk O, Bledzki AK, Fink H-P et al. (2014) Progress report on natural fiber reinforced composites. *Macromolecular Materials and Engineering* **299**(1): 9–26, [10.1002/mame.201300219](https://doi.org/10.1002/mame.201300219).
- Gholampour A and Ozbakkaloglu T (2020) A review of natural fiber composites: properties, modification and processing techniques, characterization, applications. *Journal of Materials Science* **55**(3): 829–892, [10.1007/s10853-019-03951-0](https://doi.org/10.1007/s10853-019-03951-0).
- Faheed NK (2024) Advantages of natural fiber composites for biomedical applications: a review of recent advances. *Emergent Materials* **7**(1): 63–75, [10.1007/s42247-024-00312-7](https://doi.org/10.1007/s42247-024-00312-7).
- Bledzki A, Reihmane S and Gassan J (1996) Properties and modification methods for vegetable fibers for natural fiber composites. *Journal of Applied Polymer Science* **59**(8): 1329–1336, [10.1002/\(SICI\)1097-4628\(19960223\)59:8](https://doi.org/10.1002/(SICI)1097-4628(19960223)59:8).

5. Thanikodi S, Rathinasamy S and Solairaju JA (2025) Developing a model to predict and optimize the flexural and impact properties of jute/kenaf fiber nano-composite using response surface methodology. *The International Journal of Advanced Manufacturing Technology* **136(1)**: 195–209, [10.1007/s00170-025-09714-3](https://doi.org/10.1007/s00170-025-09714-3).
6. Palanisamy S et al. (2024) Selection and processing of natural fibers and nanocellulose for biocomposite applications: a brief review. *BioResources* **19(1)**, [10.15376/biores.19.1.1-12](https://doi.org/10.15376/biores.19.1.1-12).
7. Sun Z (2018) Progress in the research and applications of natural fiber-reinforced polymer matrix composites. *Science and Engineering of Composite Materials* **25(5)**: 835–846, [10.1515/secm-2017-0272](https://doi.org/10.1515/secm-2017-0272).
8. Bera T and Mohanty S (2025) Implementation of Taguchi design for dry sliding wear of high-density polyethylene/silicon carbide composite. *Materialwissenschaft Und Werkstofftechnik* **56(2)**: 226–234, [10.1002/mawe.202400113](https://doi.org/10.1002/mawe.202400113).
9. Hisam MW, Dar AA, Elrasheed MO et al. (2024) The versatility of the Taguchi method: optimizing experiments across diverse disciplines. *Journal of Statistical Theory and Applications* **23(4)**: 365–389, [10.1080/15366367.2023.2247128](https://doi.org/10.1080/15366367.2023.2247128).
10. Islam T, Chaion MH, Jalil MA et al. (2024) Advancements and challenges in natural fiber-reinforced hybrid composites: a comprehensive review. *SPE Polymers* **5(4)**: 481–506, [10.1002/spe.1384](https://doi.org/10.1002/spe.1384).
11. Liu D, Zhang Y, Sun X et al. (2014) Recent advances in bio-sourced polymeric carbohydrate/nanotube composites. *Journal of Applied Polymer Science* **131(12)**, [10.1002/app.40359](https://doi.org/10.1002/app.40359).
12. Samouh Z, et al. (2023). Investigation on bio-sourced textile reinforcement for composite material based on sisal Moroccan yarns. In *IOP Conference Series: Materials Science and Engineering*. IOP Publishing.
13. Yi X-S, Zhang X, Ding F et al. (2018) Development of bio-sourced epoxies for bio-composites. *Aerospace* **5(2)**: 65, [10.3390/aerospace5020065](https://doi.org/10.3390/aerospace5020065).
14. Stokke DD, Wu Q and Han G (2013) *Introduction to Wood and Natural Fiber Composites*. John Wiley & Sons.
15. Saada K, Amroune S, Belaadi A et al. (2024) Enhancing the mechanical characteristics of eco-friendly composite materials: Taguchi and RSM optimization. *Journal of Natural Fibers* **21(1)**: 2427704, [10.1080/15440478.2024.2427704](https://doi.org/10.1080/15440478.2024.2427704).
16. Saheb DN and Jog JP (1999) Natural fiber polymer composites: a review. *Advances in polymer technology. Journal of the Polymer Processing Institute* **18(4)**: 351–363, [10.1002/\(SICI\)1098-2329\(199912\)18:4](https://doi.org/10.1002/(SICI)1098-2329(199912)18:4).
17. Sumesh K et al. (2024) Mechanical properties of ramie/flax hybrid natural fiber composites under different conditions. *Biomass Conversion and Biorefinery* **14(23)**: 29579–29590, [10.1007/s13399-024-03059-5](https://doi.org/10.1007/s13399-024-03059-5).
18. Aslan M, Tufan M and Küçükömeroğlu T (2018) Tribological and mechanical performance of sisal-filled waste carbon and glass fibre hybrid composites. *Composites Part B: Engineering* **140**: 241–249, [10.1016/j.compositesb.2018.01.027](https://doi.org/10.1016/j.compositesb.2018.01.027).
19. Hu W, Zhang D, Ftwi E et al. (2023) Development of sustainable low carbon engineered cementitious composites with waste polyethylene fiber, sisal fiber and carbonation curing. *Resources, Conservation and Recycling* **197**: 107096, [10.1016/j.resconrec.2023.107096](https://doi.org/10.1016/j.resconrec.2023.107096).
20. Sosiati H, et al. (2022). The influence of carbon fiber content on the tensile, flexural, and thermal properties of the sisal/PMMA composites.
21. Joseph K, Tolêdo Filho RD, James B et al. (1999) A review on sisal fiber reinforced polymer composites. *Revista Brasileira de Engenharia Agrícola e Ambiental* **3(3)**: 367–379, [10.1590/S1415-43662099000300007](https://doi.org/10.1590/S1415-43662099000300007).
22. Jagadeesh P, Puttegowda M, Suyambulingam I et al. (2024) Analysis of friction and wear performance of eco-friendly basalt filler reinforced polylactic acid composite using the Taguchi approach. *Journal of Thermoplastic Composite Materials* **37(7)**: 2479–2504, [10.1177/08927057221104576](https://doi.org/10.1177/08927057221104576).
23. Jagannath GRR, Naik Narayana CK, Hulikere Mallaradhya M et al. (2024) Enhancing wear resistance of UHMWPE composites with micro MoS₂ and nano graphite: a Taguchi-DOE approach. *ACS Omega* **9(14)**: 16743–16758, [10.1021/acsomega.4c01680](https://doi.org/10.1021/acsomega.4c01680).
24. Noorunnisa Khanam P, Abdul Khalil HPS, Jawaid M et al. (2010) Sisal/carbon fibre reinforced hybrid composites: tensile, flexural and chemical resistance properties. *Journal of Polymers and the Environment* **18(4)**: 727–733, [10.1007/s10924-010-0245-4](https://doi.org/10.1007/s10924-010-0245-4).
25. Reyes-Mayer A and Romo-Urbe A (2025) Single layer woven carbon fibers improved the thermal and mechanical properties of epoxy resin. *Emerging Materials Research, I–33* **14(2)**: 119–131, [10.1680/jemmr.23.00190](https://doi.org/10.1680/jemmr.23.00190).
26. Cavalcanti DKK, Banea MD, Neto JSS et al. (2019) Mechanical characterization of intralaminar natural fibre-reinforced hybrid composites. *Composites Part B: Engineering* **175**: 107149, [10.1016/j.compositesb.2019.107149](https://doi.org/10.1016/j.compositesb.2019.107149).
27. El-Tayeb N (2008) Tribo-characterization of natural fibre-reinforced polymer composite material. *Proceedings of the Institution of Mechanical Engineers, Part J: Journal of Engineering Tribology* **222(7)**: 935–946, [10.1243/13506501JET430](https://doi.org/10.1243/13506501JET430).
28. Hull D (1998) *An Introduction to Composite Materials* (2nd. ed.). Cambridge University Press.
29. Ibrahem R (2020) Effect of molybdenum disulfide nano-particles on dry sliding behavior of carbon fiber reinforced epoxy. *Tribology in Industry* **42(1)**: 115–122, [10.24874/ti.855.12.19.02](https://doi.org/10.24874/ti.855.12.19.02).
30. Mallick PK (2007) *Fiber-Reinforced Composites: Materials, Manufacturing, and Design* 3rd ed., CRC Press, [10.1201/9781420005981](https://doi.org/10.1201/9781420005981).
31. Naveen J, et al. (2019) Mechanical and physical properties of sisal and hybrid sisal fiber-reinforced polymer composites. In *Mechanical and Physical Testing of Biocomposites, Fiber-Reinforced Composites and Hybrid Composites* (Jawaid M, Thariq M, and Saba N (eds)). Elsevier, pp. 427–440, [10.1016/B978-0-08-102292-4.00025-2](https://doi.org/10.1016/B978-0-08-102292-4.00025-2).
32. Pihtili H (2009) An experimental investigation of wear of glass fibre–epoxy resin and glass fiber–polyester resin composite materials. *European Polymer Journal* **45(1)**: 149–154, [10.1016/j.eurpolymj.2008.10.007](https://doi.org/10.1016/j.eurpolymj.2008.10.007).
33. Soni A, Das PK, Gupta SK et al. (2024) An overview of recent trends and future prospects of sustainable natural fiber-reinforced polymeric composites for tribological applications. *Industrial Crops and Products* **222**: 119501, [10.1016/j.indcrop.2023.119501](https://doi.org/10.1016/j.indcrop.2023.119501).
34. Ramaiah G, Simeno Z, Negawo TA et al. (2025) Extraction of ensete fibers and its woven fabric green composite development for ceiling board applications. *Industrial Crops and Products* **223**: 120189, [10.1016/j.indcrop.2024.120189](https://doi.org/10.1016/j.indcrop.2024.120189).
35. Ramaiah G, Asfaw D, Mekonnen S, Tesfay W and Solomon E (2022) November) Shear thickening fluids, nano-polymer materials and their application methods for textile substrates. In. *Materials Science Forum* **1073**: 81–90, [10.4028/p-1hf4ev](https://doi.org/10.4028/p-1hf4ev).
36. Ramaiah G, Tilahun A, Negawo TA et al. (2024) Development of green composite utilizing sisal strands and sustainable 3-D printed PLA layers. *Textile & Leather Review* **7**: 938–970, [10.31881/TLR.2024.076](https://doi.org/10.31881/TLR.2024.076).
37. Ramaiah GB (2021) Theoretical analysis on applications aspects of smart materials and internet of things (IoT) in textile technology. *Materials Today: Proceedings* **45**: 4633–4638, [10.1016/j.matpr.2020.11.741](https://doi.org/10.1016/j.matpr.2020.11.741).

AQ: ?



-
38. Heim F (2024) Coating, nanoparticles, microcapsules: additive based strategies to enhance material properties. *Emerging Materials Research* **13**(4): 302, [10.1680/jemmr.2024.13.4.302](https://doi.org/10.1680/jemmr.2024.13.4.302).
39. Kumar RV et al. (2024) Taguchi analysis for wear characteristics of Al6063 alloy–zirconium silicate composites. *Journal of The Institution of Engineers (India): Series D*: 1–16, [10.1007/s40033-024-00140-1](https://doi.org/10.1007/s40033-024-00140-1).
40. Nikzad MH, Heidari-Rarani M and Mirkhalaf M (2025) A novel Taguchi-based approach for optimizing neural network architectures: application to elastic short fiber composites. *Composites Science and Technology* **259**: 110951, [10.1016/j.compscitech.2025.110951](https://doi.org/10.1016/j.compscitech.2025.110951).
41. Tuna S (2025) Optimization of parameters on fig leaf powders added polylactic acid-based composite films using Taguchi method. *Journal of Thermal Analysis and Calorimetry* 1–17, [10.1007/s10973-025-10132-7](https://doi.org/10.1007/s10973-025-10132-7).
42. Veeranjanyulu I, Haripriya V, Saminathan R et al. (2024) Friction and wear optimization of SiC/graphite reinforced AZ31 hybrid composite using Taguchi method. *International Journal on Interactive Design and Manufacturing (IJIDeM)* **18**(3): 1373–1386, [10.1007/s12008-024-00431-5](https://doi.org/10.1007/s12008-024-00431-5).
43. Sgriccia N, Hawley M and Misra M (2008) Characterization of natural fiber surfaces and natural fiber composites. *Composites Part A: Applied Science and Manufacturing* **39**(10): 1632–1637, [10.1016/j.compositesa.2008.06.006](https://doi.org/10.1016/j.compositesa.2008.06.006).
44. Sathish T, Giri J, R S and Makki E (2024) Sisal and jute composite containing carbon nanotubes for improved mechanical and thermal performance. *AIP Advances* **14**(3), [10.1063/5.0007536](https://doi.org/10.1063/5.0007536).
45. Sanjay MR, Arpitha GR, Naik LL et al. (2016) Applications of natural fibers and its composites: an overview. *Natural Resources* **07**(03): 108–114, [10.4236/nr.2016.73012](https://doi.org/10.4236/nr.2016.73012).

How can you contribute?

To discuss this paper, please submit up to 500 words to the journal office at support@emerald.com. Your contribution will be forwarded to the author(s) for a reply and, if considered appropriate by the editor-in-chief, it will be published as a discussion in a future issue of the journal.

ICE Science journals rely entirely on contributions from the field of materials science and engineering. Information about how to submit your paper online is available at www.emeraldgroupublishing.com/journal/jemmr, where you will also find detailed author guidelines.

AUTHOR QUERIES

AUTHOR PLEASE ANSWER ALL QUERIES

1

AQau— Please confirm the given-names and surnames are identified properly by the colours.

■=Given-Name, ■= Surname The colours are for proofing purposes only. The colours will not appear online or in print.

AQ1—Per the ICE Science style, the length of the abstract should be between 150 and 200 words.

Please shorten the length of this abstract to adhere to the style.

AQ2—Please define the abbreviation “PAN”.

AQ3—Please note that to ensure sequential order we have renumbered the references. Check for correctness.

AQ4—Please provide missing citation(s) for Figure 12.